Theoretical study of *i*-Process contribution to the post-AGB star IRAS 14325-6428*

Guo Li,[1,2] Jian-Rong Shi,[1,2,†] Su-Ya-La-Tu Zhang,[3,4,‡] Hong-Liang Yan,[1,2,§] and Yong-Shou Chen[5]

[1]*CAS Key Laboratory of Optical Astronomy, National Astronomical Observatories, Chinese Academy of Sciences, Beijing 100101, China*
[2]*School of Astronomy and Space Science, University of Chinese Academy of Sciences, Beijing 100049, China*
[3]*College of Physics and Electronics, and Institute of Nuclear Physics, Inner Mongolia Minzu University, Tongliao 028043, China*
[4]*Inner Mongolia Joint Key Laboratory of Nuclear and Radiation Detection, Tongliao 028043, China*
[5]*China Institute of Atomic Energy, Beijing 102413, China*

The post-asymptotic giant branch (post-AGB) star IRAS 14325-6428 exhibits a peculiar heavy-element abundance pattern, characterized by a high [Ba/La] ratio and an anomalous odd-isotope Ba ratio ($f_{\rm odd,Ba}$ = 0.25 ± 0.08), which is difficult to explain via the classical slow neutron-capture process (*s*-process). In this work, we theoretically investigate this abundance pattern by considering intermediate neutron-capture process (*i*-process) nucelosyntheis. We employ a self-consistent computational framework. A stellar model representative of the progenitor (1.5 $M_\odot$, Z = 0.003) is evolved with MESA to the thermally pulsing AGB phase to obtain intershell elemental abundances. These values are then used as input for *i*-process nucleosynthesis calculations performed with a one-zone network (NucNet Tools) at constant temperature and density. The observed heavy-element abundances are best reproduced by a model with neutron density $N_n = 5 \times 10^{13}$ cm^{-3} and neutron exposure τ = 1.4 mbarn^{-1}, followed by dilution with a scaled-solar composition. This model reproduces the high [Ba/La] and [Ba/Ce] ratios and yields a post-dilution odd-isotop fraction $f_{\rm odd,Ba} \approx 0.51$, consistent with the observational trend. The abundance pattern arises from the *i*-process path approaching the neutron magic number N = 82, where the flow slows and the material accumulates at ^{135}I, which subsequently β^--decays to ^{135}Ba. This leads to enhanced Ba production and reduced synthesis of heavier species. These results, consistent with the star's multi-element classification as enriched in both *s*- and *r*-process elements, provide quantitative support for an *i*-process origin of the heavy elements in IRAS 14325−6428, likely triggered by a relatively short-lived proton-ingestion episode in its AGB progenitor.

Keywords: post-AGB stars — nucleosynthesis — stars: abundances — stars: evolution — stars: individual (IRAS 14325-6428) — nuclear reactions, nucleosynthesis, abundances.

I. INTRODUCTION

The origin of elements heavier than iron in the universe is primarily governed by neutron capture nucleosynthesis processes[1]. Traditionally, slow (*s*-) and rapid (*r*-) neutron capture processes have been considered the two dominant mechanisms responsible for the production of heavy elements. These processes are distinguished by their characteristic neutron densities, which determine the competition between neutron capture and β-decay [2], thus setting the nucleosynthesis path on the nuclide chart and shaping the resulting abundance distributions. The *r*-process occurs at extremely high neutron densities ($N_n > 10^{20}$ cm^{-3})[3] and is associated with explosive astrophysical environments, such as neutron-star mergers [4–9] and magnetohydrodynamically driven supernovae or collapsars [10–16]. It is responsible for the synthesis of elements such as Eu, Os, Au, and Pt. In contrast, the *s*-process operates at much lower neutron densities ($N_n < 10^{11}$ cm^{-3}), mainly in asymptotic giant branch (AGB) stars [17–23] and during core He burning in massive stars [24–27], producing elements such as Sr, Y, Zr, Ba, La, Ce, and Pb.

The concept of an intermediate neutron-capture process (hereafter *i*-process), operating at neutron densities ($N_n \approx 10^{12}$–10^{20} cm^{-3}) between those of the classical slow (s-) and rapid (*r*-) processes, was originally introduced by Cowan & Rose[28]. Recent renewed and significant interest in this process stems from the growing number of observed stars whose abundance patterns cannot be satisfactorily reproduced by canonical s- or *r*-process nucleosynthesis, nor by a simple combination of these two processes. Instead, the chemical signatures of these so-called *r/s* stars are successfully matched by *i*-process models [29–32].

A prime example is the carbon-enhanced metal-poor stars that exhibit simultaneous enhancements in both *s*- and *r*-process elements (CEMP-s/r). These stars show significant over-abundances of the canonical s-process indicator Ba and the *r*-process indicator Eu (e.g. [Ba/Fe] > 1, [Eu/Fe] > 1, and [Ba/Eu] > 0; [33]). If their carbon- and *s*-process enhancements are attributed to mass transfer from a binary AGB companion, the origin of the concurrent Eu excess remains unexplained. Hypotheses involving separate pollution events from different *s*- and *r*-process sites have been found unsuccessful [34–37]. In contrast, *i*-process simulations have been shown to naturally reproduce the full heavy-element abundance patterns of CEMP-s/r stars [33, 38–41]. Another important example comes from post-AGB stars, which bear the

* This work was supported by the Strategic Priority Research Program of Chinese Academy of Sciences (No. XDB1160101), the National Key R&D Programs of China (No. 2024YFA1611903), and the National Natural Science Foundation of China (Grants Nos. 12373036 and 12465024). H.Y. acknowledges supports from the Youth Innovation Promotion Association of the CAS.
† Corresponding author, Jian-Rong Shi, sjr@bao.ac.cn
‡ Corresponding author, Su-Ya-La-Tu Zhang,zsylt0416@163.com
§ Corresponding author, Hong-Liang Yan, hlyan@nao.cas.cn

chemical imprint of their preceding AGB evolution, provide another line of evidence. Observations of post-AGB stars in the Small and Large Magellanic Clouds (SMC and LMC) reveal heavy-element enhancements. However, standard AGB stellar models corresponding to their inferred masses and metallicities tend to overpredict the abundance of Pb compared to observational upper limits [43, 44]. Lugaro et al.[45] suggested that these abundance patterns might be better explained by *i*-process nucleosynthesis, a notion quantitatively supported by the one-zone *i*-process models of Hampel et al.[38], which successfully match the observed heavy-element enhancements without overproducing Pb. Further support comes from the unique case of Sakurai's Object, a post-AGB star exhibiting extreme overabundances of first s-process peak elements like Rb, Sr, and Y. This peculiar signature is interpreted as the result of *i*-process nucleosynthesis activated during a very late thermal pulse (VLTP; [46, 47]).

The intermediate neutron densities required for the *i*-process are primarily generated by the reaction ^{13}C$(\alpha, n)^{16}$O as in the *s*-process, but under specific conditions that trigger a neutron burst. This burst is typically triggered by a proton-ingestion episode (PIE), where protons are entrained into He-burning driven convective layers rich in He and C. Within this high-temperature environment ($T > 10^8$ K), the reaction chain ^{12}C$(p,\gamma)^{13}$N$(\beta^+\nu)^{13}$C$(\alpha, n)^{16}$O is activated, rapidly generating neutron densities of the order of $N_n \approx 10^{12}$–10^{20} cm^{-3} [39, 46, 48, 49]. A diversity of astrophysical sites capable of hosting such PIEs, and by extension the *i*-process, have been proposed. The range of astrophysical sites capable of PIEs has been systematically listed by Choplin et al. [39]. Their series of works has quantitatively explored PIEs in low-metallicity, low-mass AGB models, and investigated the effects of the extra mixing scheme (overshoot, [41]) and rotation [42]. Notably, including overshoot mixing at the top of the convective thermal pulse significantly expands the range of stellar masses and metallicities for which PIEs can occur. Under certain overshoot parameters, PIE may even be possible at nearly solar metallicity [41]. It is important to note, however, that these multi-zone stellar models can show discrepancies in reproducing the observed abundances of the first *s*-process peak elements (e.g., Y, Zr) in post-AGB stars [41]. In contrast, the one-zone *i*-process framework employed by Hampel et al. [33, 38] adopts a constant temperature, density, and neutron density. Although this approach does not simulate the dynamic stellar structure of a PIE event, it provides a powerful tool to isolate and study the details of heavy-element nucleosynthesis pathways under controlled *i*-process conditions.

In the classical *s*-process, the characteristic abundance peaks are formed at isotopes with magic neutron numbers. Specifically, the second peak is dominated by the stable bottleneck isotopes ^{138}Ba, ^{139}La, and ^{140}Ce, which all have the magic neutron number $N = 82$. In contrast, the much higher neutron densities of the *i*-process shift the nucleosynthesis path away from stability. This moves the $N = 82$ bottleneck to lighter isotopes, mainly the neutron-rich, unstable ^{135}I. Its subsequent β^- decay significantly enhances ^{135}Ba production, while the bottleneck strongly suppresses the synthesis of heavier elements like La and Ce. This mechanism naturally yields the distinct signature of elevated [Ba/La] and [Ba/Ce] ratios, which cannot be reproduced by standard *s*-process models and acts as a direct observational tracer of *i*-process nucleosynthesis,and has been proposed as a possible origin of the Ba excess observed in open clusters [29]. To move from this diagnostic potential to precise physical understanding, quantitative constraints from individual, well-characterized stars are essential. The post-AGB star IRAS 14325−6428 is a prime target for such a study. It exhibits both a high [Ba/La] ratio and an anomalous Ba odd-isotope ratio ($f_{\rm odd,Ba}$[5]) [50],providing two independent and strong constraints that make it an ideal laboratory for quantitative studies of the *i*-process. This work aims to establish a self-consistent computational framework—linking stellar evolution to nucleosynthesis—to quantitatively fit the heavy-element abundances of IRAS 14325−6428, determine its optimal *i*-process parameters, and elucidate the origin of its anomalous abundance features from the perspective of neutron-capture paths. Thereby, we seek to provide a robust *i*-process interpretation for the heavy-element enrichment history of this star.

This paper is organized as follows. In Section II, we present the observed heavy-element abundance anomalies in IRAS 14325−6428 and compare them with standard *s*-process models. Section III details our self-consistent computational method, which combines stellar evolution modeling with MESA and one-zone *i*-process nucleosynthesis calculations. Our main results, including the best-fitting *i*-process parameters, the analysis of neutron-capture paths, and the diagnostic implications of the Ba odd-isotope ratio, are presented and discussed in Section IV. Finally, we summarize our findings and conclusions in Section V.

II. HEAVY ELEMENT ABUNDANCE ANOMALIES IN IRAS 14325−6428

IRAS 14325−6428 is a post-AGB star, and the abundances of some elements have been measured by De Smedt et al. [51] and Tian et al. [50]. The latter study gave a metallicity of [Fe/H]= -0.75 ± 0.05, corresponding to Z = 0.0025. The abundances of elements heavier than Fe are listed in Table 1 and plotted in Figure 1. The local thermodynamic equilibrium (LTE) results from the two measurements are relatively close. However, the Nd abundance measured by Tian et al. [50] is 0.61 dex lower than that of De Smedt et al. [51]. This difference is attributed to the adoption of different log gf values and the differences in equivalent widths caused by the placement of the continuum. For the key neutron-capture elements Ba and Eu, the non-local thermodynamic equilibrium (NLTE) corrections increase the abundances by 0.62 and 0.43 dex, respectively, compared to their LTE values. In particular, the abundance of Eu is sensitive to the adopted atomic

[5] $f_{\rm odd,Ba} = [N(^{135}{\rm Ba}) + N(^{137}{\rm Ba})]/N({\rm Ba})$.

data: if the gf value for the Eu II line at 4129 Å is taken from the NIST database instead of DeSmedt et al. [51], the resulting NLTE [Eu/Fe] drops to approximately 0.3 dex.

Table 1. The Abundances of Elements Heavier than Fe in the Star IRAS 14325-6428.

Z	Species (dex)	[X/Fe]^a	σ (dex)	[X/Fe]^b	σ
26	Fe I	0.00	0.05	0.00	0.04
26	Fe II	0.00	0.07	0.00	0.04
28	Ni I	0.12	0.06	0.12	0.08
28	Ni II	0.11	0.03	0.08	0.10
30	Zn I	0.13	0.14	...	...
38	Sr I	<1.80	...	...	...
39	Y II	1.41	0.05	1.34	0.26
40	Zr II	1.15	0.12	1.16	0.16
56	Ba II(LTE)	1.46	0.06	1.48	0.42
56	Ba II(NLTE)	2.08	0.02	...	...
57	La II	1.18	0.10	1.31	0.35
58	Ce II	1.16	0.14	1.27	0.35
60	Nd II	0.78	0.10	1.39	0.40
62	Sm II	1.33	0.13	1.35	0.41
63	Eu II(LTE)	0.82	0.14	0.79	0.41
63	Eu II(NLTE)	1.25	0.13	...	...
64	Gd II	...	...	1.25	0.34
66	Dy II	...	...	0.94	0.39
71	Lu II	...	...	1.31	0.28
72	Hf II	...	...	1.24	0.25
82	Pb II	...	...	< 2.60	...

^{a} Tian et al.[50]. ^{b} De Smedt et al.[51].

We compare the observed heavy-element pattern with predictions from AGB stellar evolutionary models in the FRUITY (FUll-Network Repository of Updated Isotopic Tables & Yields) database [21, 52–59]. For IRAS 14325−6428, with an estimated initial mass of 1.5 – 2 $M_\odot$ [60] and metallicity $Z \approx 0.0025$, we select FRUITY models of 1.5 $M_\odot$ and 2.0 $M_\odot$ with $Z = 0.003$. Their surface abundances after the last third dredge-up (TDU) are shown in Figure 1. The labels 'ST' and 'EXT' denote a standard and an extended ^{13}C pocket, respectively [53].

The M1.5Z3m3-ST model underestimates the first s-process peak (Sr, Y, Zr) and significantly underproduces Ba compared to the NLTE measurement. The M2Z3m3-ST model matches better the elements in the first-peak and approaches the observed NLTE abundance of Ba, however, it over-predicts La, Ce, Nd, and especially Hf (by > 0.5 dex). Models with an extended ^{13}C pocket ('EXT') produce higher overall heavy-element abundances. Consequently, the M2Z3m3-EXT model, which shows the highest yields and the closest match to the NLTE Ba value, further exacerbates the overproduction of elements from La to Hf seen in the M2Z3m3-ST model. It should be noted that the s-process occurring in the ^{13}C pocket of low-mass AGB star models typically enhances the second s-process peak elements (Ba, La, Ce) simultaneously, with Ce being the most enhanced. In contrast, IRAS 14325−6428 exhibits the NLTE Ba abundance that is significantly higher than those of La and Ce, a pattern that standard s-process models fail to reproduce.

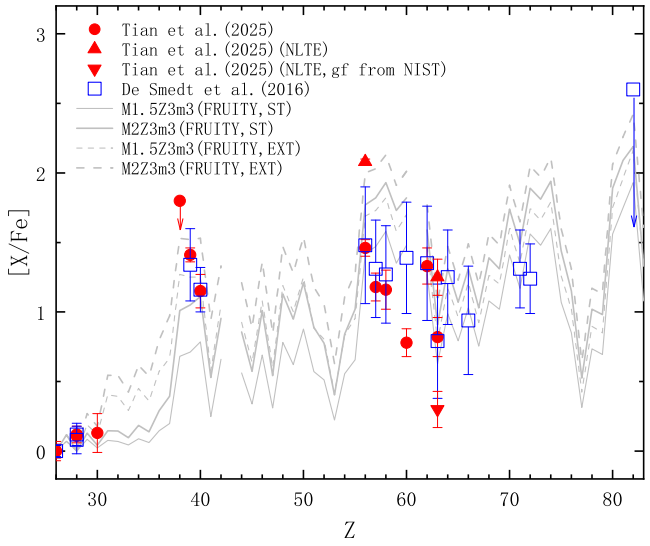

Fig. 1. Abundances of elements heavier than Fe for IRAS 14325−6428 as a function of atomic number Z. The red circles denote the LTE results from Tian et al. [50]; the red upward-pointing triangles represent their NLTE results for Ba and Eu (for Eu, the gf value of the Eu II line at 4129 Å is adopted from De Smedt et al. [51]; the red downward-pointing triangle marks the NLTE abundance of Eu obtained using the gf value for the 4129 Å line taken directly from the NIST Atomic Spectra Database. Blue open squares show the LTE measurements from De Smedt et al. [51]. Grey lines depict AGB stellar evolutionary models from the FRUITY database [57] for stars with masses and metallicities similar to IRAS 14325−6428. Model labels indicate the initial mass (in solar masses, following M) and metallicity (following Z); for example, 'Z3m3' signifies a metallicity of Z=3×10^{-3} (i.e., 0.003).

Post-AGB stars are considered potential astrophysical sites where the i-process occurs. The recent measurement of the odd barium isotope ratio in IRAS 14325−6428, $f_{\rm odd,Ba} = 0.25 \pm 0.08$ [50], provides a direct isotopic hint that its heavy elements may originate from an i-process rather than the classical s-process. Motivated by these abundance anomalies—the high [Ba/La] and [Ba/Ce] ratios and the anomalous $f_{\rm odd,Ba}$—we proceed to test the i-process hypothesis by fitting its heavy-element abundance pattern with dedicated nucleosynthesis models.

III. ONE-ZONE i-PROCESS MODEL

We calculate the nucleosynthesis of i-process using a one-zone model under the assumption of a constant neutron density, following the methodology of Hampel et al. [33, 38]. The reaction network is solved with the `NucNet Tools` software package [61]. Our custom network file (`my_net.xml`) includes 7,852 isotopes linked by 51,395 reactions. Nuclear physics data (reaction rates, masses and decay properties) are from the JINA Reaclib database (June 2021 release) [62], converted to the required XML format using the `jina_to_webnucleo` utility.

For the thermodynamic conditions, we adopt the canonical

values used in previous *i*-process studies: $T = 1.5 \times 10^8$ K and $\rho = 1600\,\mathrm{g\,cm^{-3}}$ [33, 38]. The abundance pattern of *i*-process elements is primarily governed by the neutron density N_n and the neutron exposure τ, with neutron-capture cross sections being less temperature-sensitive than charged-particle reactions. The neutron exposure τ quantifies the integrated neutron irradiation experienced by the seed nuclei. It is defined as the time-integrated product of the neutron density N_n and the mean thermal neutron velocity v_T:

$$\tau = \int N_\mathrm{n}\, v_T\, dt = \int N_\mathrm{n} \sqrt{2k_\mathrm{B}T/m_n}\, dt, \qquad (1)$$

where k_B is the Boltzmann constant and m_n is the neutron mass.

The initial isotopic composition for the network calculation is a critical input. Unlike previous studies of one-zone *i*-processes that adopted pre-computed intershell abundances [63, 64], we generate this composition self-consistently. We use the stellar evolution code MESA (Modules for Experiments in Stellar Astrophysics) [65–70] for this purpose. MESA is a robust open-source code whose modular design, extensive physics options, and regular updates make it a versatile tool for a wide range of stellar astrophysics problems. We simulate a stellar model appropriate for the progenitor of IRAS 14325−6428, with an initial mass of $1.5\,M_\odot$ and metallicity $Z = 0.003$. The simulation uses the MESA release r24.08.1. The input physics primarily follows the setup of Huscher et al. [71], which employs scaled mixing-length and mass-loss parameters and includes a custom routine [72] to improve numerical convergence during thermal pulses. The convective boundary mixing is treated with the diffusive overshoot scheme of Herwig [73] at the bottom of the convective envelope and at the boundary of the He-burning shell. The initial composition uses the photospheric solar abundance scale of [74], supplemented where necessary with the abundances of [75] (set by `initial_zfracs = 9` in MESA). The in-built reaction network in MESA, which we use for the stellar structure and evolution calculations, is tailored for *s*-process studies. It contains 551 isotopes from H to Po, encompassing all stable isotopes and extends to radioactive species with up to approximately two neutrons beyond the most neutron-rich stable isotope for a given element. This coverage provides a sufficiently broad baseline near stability for reliably computing the intershell composition, which subsequently serves as the seed for our dedicated *i*-process network calculation. The model evolves from a pre-main sequence of uniform composition. The evolution is divided into five key phases, with control parameters adjusted as needed: (1) main sequence, (2) red giant branch, (3) horizontal branch, (4) early AGB before thermal pulses begin, and (5) the thermally pulsing AGB (TP-AGB) phase. We extract the uniformly mixed intershell material after the second thermal pulse to serve as the starting composition for the *i*-process network calculation.

To compare the model output with the observed surface heavy-element abundances of the star, the synthesized *i*-processed material is mixed with material of scaled-solar composition—a dilution controlled by a factor d (equation (2) of Hampel et al. [38]) that simulates astrophysical processes such as dredge-up or mass transfer in a binary system. The heavy-element abundance pattern obtained from our calculations is primarily influenced by the neutron density N_n and the neutron exposure τ, while d affects only the overall scaling, not the pattern's shape.

IV. RESULT AND DISCUSSIONS

The most prominent feature in the heavy-element pattern of IRAS 14325-6428 is the exceptionally high NLTE abundance of Ba relative to the subsequent elements La and Ce, resulting in large [Ba/La] and [Ba/Ce] ratios. To reproduce this signature, nucleosynthesis must be arrested at the N=82 neutron magic number. This requires a model with a relatively small neutron exposure τ, such that the neutron-capture path reaches this bottleneck but does not leak significantly beyond it to produce substantial amounts of La and Ce. Therefore, by adjusting the neutron density N_n and exposure τ, we find the best fit to the observed abundances (Figure 2) is achieved with $N_n = 5 \times 10^{13}$ cm^{-3}, $\tau = 1.4$ mb^{-1}, and a dilution factor $d = 0.9975$. This *i*-process model successfully reproduces the overall pattern, most critically matching the high NLTE Ba abundance and the abundances of La and Ce, thereby naturally explaining the high [Ba/La] and [Ba/Ce] ratios. A detailed comparison reveals that the model overpredicts Zr ($Z = 40$), while for most elements from Ba to Hf, the predictions agree with the observations within the respective measurement uncertainties of De Smedt et al. [51] (see the lower panel of Figure 2). The calculated value of Nd ($Z = 60$) is between the two measured ones, and Sm, Gd, and Dy are slightly underestimated. The Eu abundance of the model agrees with the LTE measurement. In particular, the heavier elements Lu ($Z = 71$) and Hf ($Z = 72$) are well-matched. Most importantly, unlike standard *s*-process models, our *i*-process fit self-consistently explains the key abundance anomalies, providing strong, independent theoretical support for the *i*-process origin proposed by Tian et al. [50].

To validate the analysis, Figure 3 displays the neutron-capture paths at $t = 1.78 \times 10^5$ s (corresponding to $\tau = 1.4$ mb^{-1}) for our best-fit model ($N_n = 5 \times 10^{13}$ cm^{-3}). It is evident that, unlike the *s*-process which operates close to the valley of stability, the *i*-process path at this neutron density proceeds far from stability. Due to relatively low neutron exposure ($\tau = 1.4$ mb^{-1}), the main reaction flow stagnates in the $N = 82$ neutron magic-number bottleneck, causing a pronounced pile-up of isotopes, most notably the radioactive nucleus ^{135}I and the stable ^{136}Xe. The subsequent β^--decay of ^{135}I feeds the production of ^{135}Ba, thus significantly enhancing the total abundance of Ba, while blocking the neutron-capture flow at $N = 82$ strongly suppresses the synthesis of heavier elements such as La ($Z = 57$) and Ce ($Z = 58$). This dual effect — the selective enhancement of Ba coupled with the inhibited production of La and Ce—directly explains the observed high [Ba/La] and [Ba/Ce] ratios. The dominance of the $^{135}\mathrm{I} \rightarrow {}^{135}\mathrm{Ba}$ channel also predicts an extreme odd-to-

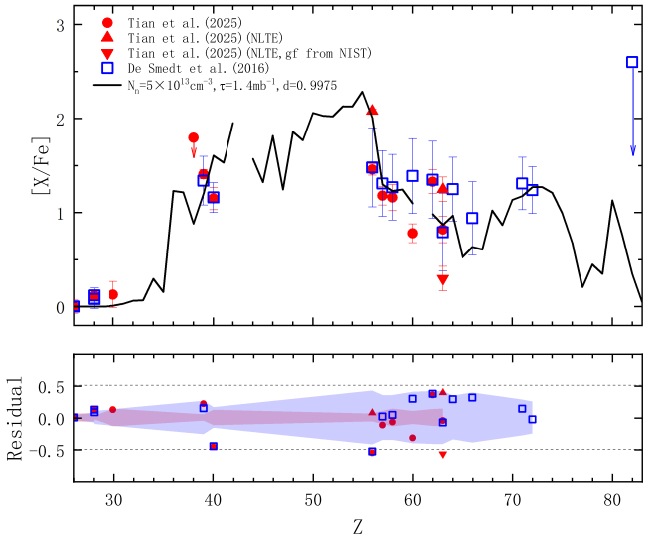

Fig. 2. The top panel compares the observational data (see Figure 1 for details) with the best-fitting *i*-process model (solid black line) for the parameters $N_n = 5 \times 10^{13}$ cm^{-3}, $\tau = 1.4$ mb^{-1}, and $d = 0.9975$. The bottom panel shows the corresponding residuals (observed − model). The red and blue shaded regions represent the observational uncertainties in the measurements of Tian et al. [50] and De Smedt et al. [51] , respectively.

even barium isotope ratio, with a pre-dilution $f_{\rm odd,Ba} = 0.96$. Even after dilution ($f_{\rm odd,Ba} = 0.51$), this value remains vastly higher than the expectation of *s*-process ($\lesssim 0.11$). Thus, Figure 3 provides the nuclear-physics foundation for the abundance anomalies and establishes $f_{\rm odd,Ba}$ as a potent diagnostic to discriminate *i*-process from *s*-process enrichment.

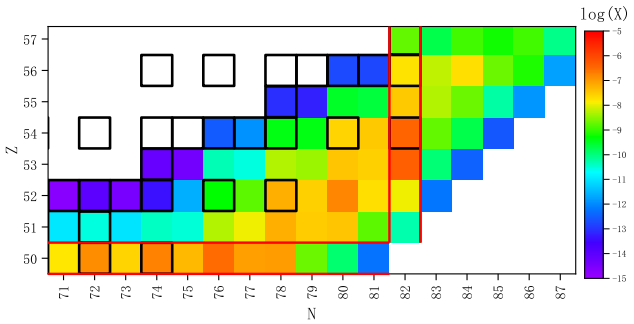

Fig. 3. Neutron-capture paths in the nuclide chart for Sn to La elements. The model parameters are $N_n = 5 \times 10^{13}$ cm^{-3}, $\tau = 1.4$ mb^{-1}, and the shown time is $t = 1.78 \times 10^5$ s (corresponding to $\tau = 1.4$ mb^{-1}). Isotope positions are determined by neutron (N) and proton (Z) numbers. Stable isotopes are highlighted with bold black borders. Magic proton number $Z = 50$ and magic neutron number $N = 82$ are marked with red boxes. Color represents the logarithm of the mass fraction $\log(X)$ for each isotope.

Figure 4 presents the results of *i*-process nucleosynthesis for a neutron density of $N_n = 5 \times 10^{13}$ cm^{-3} and a dilution factor of $d = 0.9975$. The upper panel shows the evolution of the abundances ([X/Fe]) of elements near the second *s*-process peak, from Xe to Nd, as a function of neutron exposure τ (ranging from 0.5 to 5.0 mbarn^{-1}). The abundances of these elements generally increase initially and then decrease with increasing τ, reflecting the progression of the neutron-capture path from lower mass numbers to the region of the second *s*-process peak and beyond. A clear synchronization can be seen in the evolution of the abundance of La, Ce, Pr, and Nd. In contrast, Ba reaches its maximum abundance earlier than these subsequent elements and exhibits lower abundances at higher τ values. This asynchronicity in the production of Ba relative to La, Ce, Pr, and Nd creates the potential for a high [Ba/La] ratio at low neutron exposures, as seen in the abundance pattern of IRAS 14325-6428. The lower panel shows that the [Ba/La] ratio indeed features a pronounced peak at low τ. The underlying cause for this, as mentioned earlier, is the role of ^{135}I as the main bottleneck isotope in the *i*-process, a phenomenon not present in the *s*-process where ^{138}Ba serves as the bottleneck isotope.

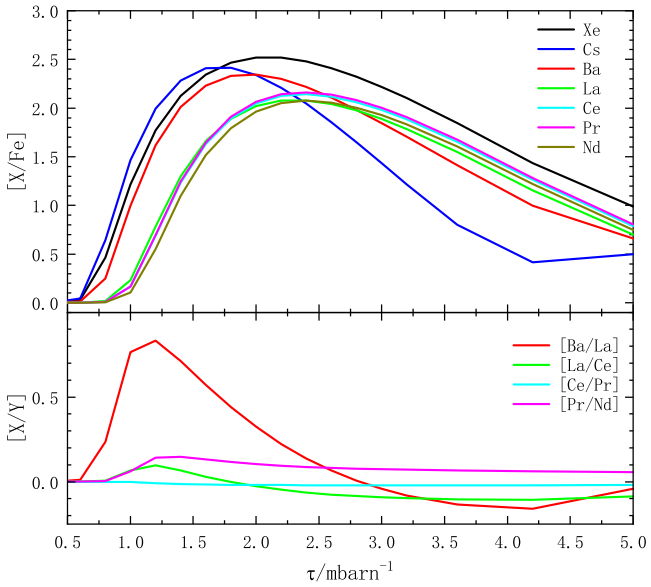

Fig. 4. Upper panel: Abundances [X/Fe] of elements from Xe to Nd as a function of neutron exposure τ for a model with a fixed neutron density of $N_n = 5 \times 10^{13}$ cm^{-3} and a dilution factor of d = 0.9975. Lower panel: Corresponding abundance ratios between adjacent elements, i.e., [Ba/La], [La/Ce], [Ce/Pr], and [Pr/Nd].

Figure 5 illustrates the effects of the *i*-process near the N = 82 shell closure, specifically its impact on the isotopic composition of Ba. The panels show, for a model with $N_n = 5 \times 10^{13}$ cm^{-3} and $d = 0.9975$, the evolution with neutron exposure τ of: the isotopic fractions f of $^{134-138}$Ba[6] (panels a, b), the odd-isotope fraction $f_{\rm odd,Ba} = f(^{135}\text{Ba}) + f(^{137}\text{Ba})$ (panel c), and the total Ba abundance (panel d). The total abundance of Ba peaks at $\tau \approx 2$ mbarn^{-1}. In the low τ case, the high Ba abundance is dominated by ^{135}Ba, produced from

[6] $f(^{134-138}\text{Ba}) = N(^{134-138}\text{Ba})/N(\text{Ba})$.

the β^--decay of the bottleneck isotope ^{135}I, which also forces $f_{\rm odd,Ba}$ to be dominated by ^{135}Ba, both for the pre- and post-dilution. This early dominance of ^{135}Ba over the magic ^{138}Ba is a distinct signature of the *i*-process, in stark contrast to the *s*-process where ^{138}Ba is produced promptly near stability. At higher τ ($\gtrsim 2.5\,{\rm mbarn}^{-1}$), the path of neutron-capture moves beyond Ba, allowing ^{138}Ba and ^{137}Ba (the latter from decay of ^{137}Cs, $t_{1/2}$ = 30 yr) to become significant. Comparison between pre- and post-dilution panels (a and b) reveals that mixing with the scaled-solar composition (where ^{138}Ba exceeds ^{135}Ba by an order of magnitude) is not a simple scaling but selectively alters the final isotopic ratios, making the dilution factor d a critical parameter in shaping the observable diagnostic $f_{\rm odd,Ba}$.

As shown in Figure 5 (c), for our best *i*-process fitting model parameters ($N_n = 5 \times 10^{13}\,{\rm cm}^{-3}$, d = 0.9975), the predicted post-dilution $f_{\rm odd,Ba}$ varies significantly with neutron exposure τ, reaching a maximum of 0.62 at τ = 1.8 mbarn^{-1}. For reference, Arlandini et al. [76] reported $f_{\rm odd,Ba}$ values of 0.11 for the pure *s*-process, 0.18 for the solar system, and 0.46 for the pure *r*-process component of the solar system. Similarly, Prantzos et al. [78] gave $f_{\rm odd,Ba} \approx 0.1$ for the *s*-process and ≈ 0.75 for the *r*-process, while Choplin et al. [77] found a range of $0.67^{+0.09}_{-0.40}$ for their *i*-process models. As previously established, our model achieves the best fit to the abundances of heavy-elements at $\tau \sim 1.4\,{\rm mbarn}^{-1}$, resulting in a post-dilution $f_{\rm odd,Ba}$ = 0.51. The observational result of Tian et al. [50] is $f_{\rm odd,Ba} = 0.25 \pm 0.08$. While the absolute values are not identical, both are unequivocally above the *s*-process baseline ($f_{\rm odd,Ba} \lesssim 0.11$), thereby robustly excluding a classical *s*-process origin. The observed value lies between the pure *s*- and *r*-process components for the solar system calculated by Arlandini et al.[76], a pattern indicative of contamination by an *i*-process. Our theoretical value, while higher than the pure *r*-process value from Arlandini et al.[76], falls comfortably within the range reported for *i*-process models by Choplin et al.[77] and remains below the *r*-process value given by Prantzos et al.[78]. Therefore, our theoretical $f_{\rm odd,Ba}$ result also provides strong support for an *i*-process origin.

Hampel et al. [38], whose calculations similarly employ a one-zone model, found characteristic neutron densities of N_n = 10^{13} to $10^{14}\,{\rm cm}^{-3}$ and exposures $\tau \gtrsim 1.8\,{\rm mbarn}^{-1}$ for CEMP-s/r stars, whereas their Pb-poor post-AGB stars required N_n = 10^{11} to $10^{12}\,{\rm cm}^{-3}$ and $1.0 \lesssim \tau \lesssim 1.3\,{\rm mbarn}^{-1}$. The best-fitting neutron density for the post-AGB star IRAS 14325−6428 in this work, $N_n = 5 \times 10^{13}\,{\rm cm}^{-3}$, is comparable to their CEMP-s/r range. This is expected: adopting the lower neutron density (N_n = 10^{11} to $10^{12}\,{\rm cm}^{-3}$) characteristic of Pb-poor post-AGB stars in Hampel et al. [38] would place the neutron-capture path much closer to the stability valley, and consequently, no choice of τ could yield the characteristically high [Ba/La] and [Ba/Ce] ratios observed in IRAS 14325−6428. Indeed, the post-AGB selected in Hampel et al. [38] do not exhibit such high ratios. In contrast, the best-fitting neutron exposure for IRAS 14325−6428 (τ = 1.4 mbarn^{-1}) is significantly lower than the CEMP-s/r range, but lies near the upper edge of the post-AGB range.

The heavy-element enrichment in a post-AGB star can be attributed to nucleosynthesis that occurred during its prior stellar evolution. The *i*-process in AGB stars is typically triggered by PIEs, where protons entrained into He- and C-rich convective layers produce high neutron densities via the $^{12}{\rm C}(p,\gamma)^{13}{\rm N}(\beta^+\nu)^{13}{\rm C}(\alpha,n)^{16}{\rm O}$ chain. The low τ for IRAS 14325−6428 may therefore indicate a weaker or shorter-lived PIE. Stellar models support this picture. For example, Choplin et al. [41], using a large nuclear network coupled to chemical transport equations and setting convective boundary overshooting above the convective pulse, showed that this allows PIEs to occur at metallicities up to [Fe/H] ≈ -0.5. The metallicity of IRAS 14325−6428 ([Fe/H] = -0.75 ± 0.05) falls within this extended range and is notably higher than that of the Pb-poor post-AGB stars in Hampel et al. [38]. It is worth noting that our best-fit N_n is comparable to the peak neutron density ($N_{n,\rm max}$) in their [Fe/H] = −0.5 models, which is the smallest in their metallicity sequence — illustrating the trend of decreasing neutron density with increasing metallicity. A similar trend is seen in models of rapidly accreting white dwarfs [79–81]. Furthermore, the existence of *i*-process-like nucleosynthesis at near-solar metallicity is evidenced by Sakurai's Object, where a PIE during a very late thermal pulse has been invoked to explain its anomalous abundances [46, 47]. Together, these studies contextualize our derived parameters and strengthen the case for an *i*-process origin in IRAS 14325−6428.

To independently assess the heavy-element pattern of IRAS 14325-6428 and to provide additional evidence for its possible *i*-process origin, we employed the multi-element diagnostic scheme developed by Karinkuzhi et al. [31]. This method quantifies a star's deviation from a pure *r*-process pattern by calculating two key distance metrics—the signed distance, d_S, and the root-mean-square distance, d_{rms} (see their Eqs. (3) & (4))—based on a suite of heavy-element abundances. The use of multiple elemental abundances makes this a more robust diagnostic than traditional two-element abundance ratios such as [Ba/Eu] or [La/Eu]. According to the calibration in that work, a star is classified as enriched in the *s*-process elements if $d_S \geq 0.6$, and as enriched in both *r*- and *s*-process elements if $d_S < 0.6$. The d_{rms} metric provides a consistent, complementary separation, with the former group typically occupying $d_{rms} \gtrsim 0.7$ and the latter in a range of $0.5 \lesssim d_{rms} < 0.8$. Applying this scheme to the measured abundances of IRAS 14325-6428, we compiled a set of heavy-element abundances ([X/Fe]) covering the range from Z = 31 (Ga) to Z = 82 (Pb), as available. For elements with overlapping measurements in the two main studies, we adopted the average value. For the critical elements Ba and Eu, we specifically employed the NLTE abundances recommended by Tian et al. [50] ([Eu/Fe] = 1.25, [Ba/Fe] = 2.08). Based on this combined abundance set, the calculated distances are d_S = 0.50 and d_{rms} = 0.67. These values place IRAS 14325-6428 unequivocally within the diagnostic range for stars enriched in both *r*- and *s*-process elements ($d_S <$ 0.6, $0.5 \lesssim d_{rms} < 0.8$). This result provides an additional, independent line of evidence supporting the *i*-process origin for the heavy elements in this star.

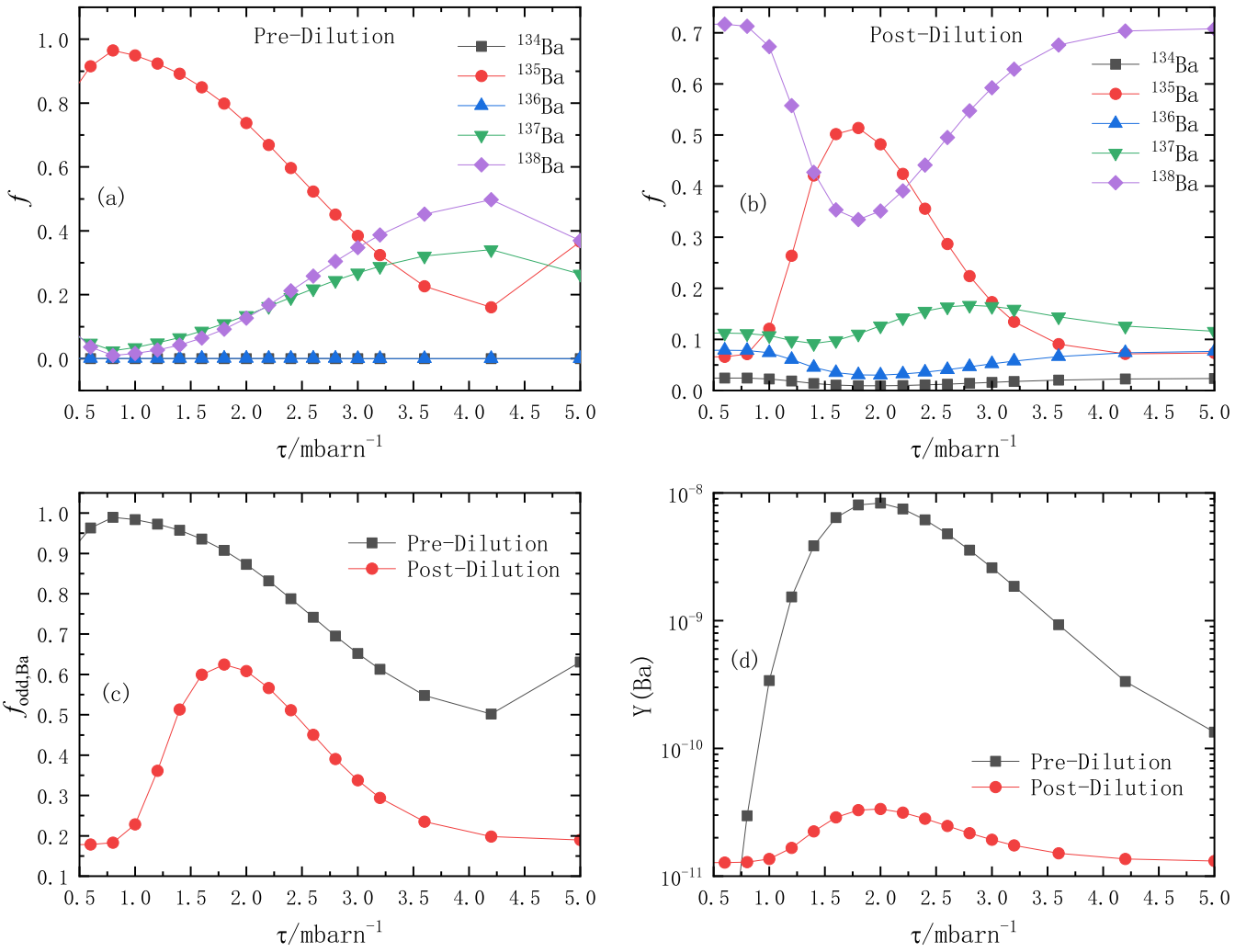

Fig. 5. Evolution of Ba isotopic fractions and total abundance as a function of neutron exposure τ for an *i*-process model with a fixed neutron density of $N_n = 5 \times 10^{13}$ cm^{-3} and a dilution factor of $d = 0.9975$. (**a**) Isotopic fractions $f(^{134-138}\mathrm{Ba}) = N(^{134-138}\mathrm{Ba})/N(\mathrm{Ba})$ pre-dilution. (**b**) Same as panel (a), but post-dilution with scaled-solar material. (**c**) The odd-isotope fraction $f_{\mathrm{odd,Ba}} = (N(^{135}\mathrm{Ba}) + N(^{137}\mathrm{Ba}))/N(\mathrm{Ba})$, shown for both pre- and post-dilution cases. (**d**) The total molar fraction of Ba, $Y(\mathrm{Ba})$, pre- and post-dilution.

V. SUMMARY

In summary, this work presents a detailed investigation on the origin of heavy elements in the post-AGB star IRAS 14325-6428. Motivated by its observed chemical peculiarities—specifically, a high [Ba/La] ratio and an anomalous barium odd-isotope ratio ($f_{\mathrm{odd,Ba}} = 0.25 \pm 0.08$)—we tested the hypothesis that its enrichment originates from the *i*-process.

We established a self-consistent computational framework linking stellar evolution to nucleosynthesis. Using the MESA code, we simulated a star with parameters comparable to IRAS 14325-6428 (1.5 $M_\odot$, $Z = 0.003$) and extracted the intershell composition after the second thermal pulse to serve as the initial abundances for the *i*-process network calculation. The nucleosynthesis was computed using a one-zone model with the `NucNet Tools` package, adopting a constant neutron density.

Our best-fit *i*-process model, with parameters $N_n = 5 \times 10^{13}$ cm^{-3}, $\tau = 1.4$ mb^{-1}, and a dilution factor $d = 0.9975$, successfully reproduces the key features of the star's heavy-element abundance pattern. The model accurately matches the high NLTE abundance of Ba and the abundances of La and Ce, resulting in the observed high [Ba/La] and [Ba/Ce] ratios. The physical cause is traced to the *i*-process path stalling at the $N = 82$ neutron magic number, leading to a pile-up of ^{135}I that decays to ^{135}Ba, thus improving Ba production while suppressing the synthesis of heavier elements such as La and Ce. This mechanism also naturally predicts a high Ba odd-isotope ratio ($f_{\mathrm{odd,Ba}} \approx 0.51$ post-dilution), consistent with the trend indicated by observations.

Furthermore, applying an independent, multi-element diagnostic scheme to the star's abundances classifies it unequivocally as enriched in both *r*- and *s*-process elements, providing additional evidence supporting an *i*-process origin.

Therefore, this study provides robust, quantitative support through detailed modeling that the heavy elements in

IRAS 14325-6428 were indeed synthesized by an *i*-process. The derived physical conditions ($N_{\rm n}, \tau$) are consistent with a scenario involving a relatively short-lived proton-ingestion episode in its AGB progenitor, offering important constraints on this nucleosynthesis pathway at moderate metallicity.

VI. BIBLIOGRAPHY

[1] A. Arcones, F.-K. Thielemann, Origin of the elements. Astron. Astrophys. Rev., **31**: 1 (2023). DOI: 10.1007/s00159-022-00146-x

[2] C. Sneden, J. J. Cowan, R. Gallino, Neutron-capture elements in the early galaxy. Annu. Rev. Astron. Astrophys., **46**, 241–288 (2008). doi: 10.1146/annurev.astro.46.060407.145207

[3] B. S. Meyer, The *r*-, *s*-, and p-processes in nucleosynthesis. Annu. Rev. Astron. Astrophys., **32**, 153–190 (1994). doi: 10.1146/annurev.aa.32.090194.001101

[4] M. Arnould, S. Goriely, K. Takahashi, The *r*-process of stellar nucleosynthesis: Astrophysics and nuclear physics achievements and mysteries. Phys. Rep., **450**, 97–213 (2007). doi: 10.1016/j.physrep.2007.06.002

[5] S. Goriely, N. Chamel, H. T. Janka, J. M. Pearson, Further explorations of Skyrme-Hartree-Fock-Bogoliubov mass formulas. XII. Stiffness and stability of neutron-star matter. Astron. Astrophys., **531**, A78 (2011). doi: 10.1051/0004-6361/201116897

[6] S. Wanajo, Y. Sekiguchi, N. Nishimura, *et al*., Production of all the R-process nuclides in the dynamical ejecta of neutron star mergers. Astrophys. J., **789**, L39 (2014). doi: 10.1088/2041-8205/789/2/L39

[7] O. Just, A. Bauswein, R. Ardevol Pulpillo, S. Goriely, H.-T. Janka, Comprehensive nucleosynthesis analysis for ejecta of compact binary mergers. Mon. Not. R. Astron. Soc., **448**, 541–567 (2015). doi: 10.1093/mnras/stv009

[8] K. F. Thielemann, M. Eichler, I. V. Panov, B. Wehmeyer, Neutron star mergers and nucleosynthesis of heavy elements. ARNPS, **67**, 253 (2017). doi: 10.1146/annurev-nucl-102115-044819

[9] B. Côté, C. L. Fryer, K. Belczynski, *et al*., The origin of *r*-process elements in the Milky Way. Astrophys. J., **855**, 99 (2018). doi: 10.3847/1538-4357/aaad67

[10] C. Winteler, R. Käppeli, A. Perego, *et al*., Magnetorotationally driven supernovae as the origin of early galaxy *r*-process elements? Astrophys. J. Lett., **750**, L22 (2012). doi: 10.1088/2041-8205/750/1/L22

[11] N. Nishimura, H. Sawai, T. Takiwaki, S. Yamada, F.-K. Thielemann, The *r*-process nucleosynthesis in the various jet-induced supernovae. Astrophys. J. Lett., **836**, L21 (2017). doi: 10.3847/2041-8213/aa5dee

[12] N. Nishimura, T. Takiwaki, F.-K. Thielemann, The *r*-process nucleosynthesis in the various jet-like explosions of magnetorotational core-collapse supernovae. Astrophys. J., **810**, 109 (2015). doi: 10.1088/0004-637X/810/2/109

[13] D. M. Siegel, J. Barnes, B. D. Metzger, Collapsars as a major source of *r*-process elements. Nature, **569**, 241–244 (2019). doi: 10.1038/s41586-019-1136-0

[14] Z. He, T. Kajino, M. Kusakabe, *et al.*, Possibility of secondary *i*- and *s*-processes following *r*-process in the collapsar jet. Astrophys. J. Lett., **966**, L37 (2024). doi: 10.3847/2041-8213/ad444c

[15] Z. He, Y. Lin, Y. Luo, T. Kajino, H. Li, Rare earth element nucleosynthesis in collapsars: Sensitivity to (n,γ) reaction rates of unstable isotopes during secondary *i*- and *s*-processes. Astrophys. J., **1000**, 177 (2026). doi: 10.3847/1538-4357/ae4739

[16] M. Ono, M. Hashimoto, S. Fujimoto, K. Kotake, S. Yamada, Effects of rotation on *r*-process nucleosynthesis in magneto-hydrodynamic jet of core-collapse supernovae. Prog. Theor. Phys., **128**, 741–757 (2012). doi: 10.1143/PTP.128.741

[17] R. Gallino, C. Arlandini, M. Busso, *et al*., Evolution and nucleosynthesis in low-mass asymptotic giant branch stars. II. Neutron capture and the *s*-process. Astrophys. J., **497**, 388–403 (1998). doi: 10.1086/305437

[18] F. Herwig, Evolution and nucleosynthesis of asymptotic giant branch stars. Annu. Rev. Astron. Astrophys., **43**, 435–479 (2005). doi: 10.1146/annurev.astro.43.072103.150600

[19] S. Cristallo, L. Piersanti, O. Straniero, *et al.*, The FRUITY database: A stellar evolution portal for nucleosynthesis. Pub. Astron. Soc. Aust., **26**, 139–150 (2009). doi: 10.1071/AS08024

[20] S. Cristallo, O. Straniero, R. Gallino, *et al.*, Evolution, nucleosynthesis, and yields of low-mass asymptotic giant branch stars at different metallicities. Astrophys. J., **696**, 797–820 (2009). doi: 10.1088/0004-637X/696/1/797

[21] S. Cristallo, L. Piersanti, O. Straniero, *et al.*, Evolution, nucleosynthesis, and yields of AGB stars at different metallicities. II. The FRUITY database. Astrophys. J., Suppl. Ser., **197**, 17 (2011). doi: 10.1088/0067-0049/197/2/17

[22] S. Bisterzo, R. Gallino, O. Straniero, S. Cristallo, F. Käppeler, The *s*-process in low-mass asymptotic giant branch stars: A new approach to constrain the 13C-pocket. Mon. Not. R. Astron. Soc., **418**, 284–319 (2011). doi: 10.1111/j.1365-2966.2011.19484.x

[23] A. I. Karakas, J. C. Lattanzio, The Dawes Review 2: Nucleosynthesis and stellar yields of low- and intermediate-mass single stars. Pub. Astron. Soc. Aust., **31**, e030 (2014). doi: 10.1017/pasa.2014.21

[24] N. Langer, J.-P. Arcoragi, M. Arnould, On the *s*-process in massive stars. Astron. Astrophys., **210**, 187–198 (1989).

[25] N. Prantzos, M. Hashimoto, K. Nomoto, The *s*-process in massive stars: yields as a function of stellar mass and metallicity. Astron. Astrophys., **234**, 211–229 (1990).

[26] M. Pignatari, R. Gallino, G. Meynet, *et al.*, The *s*-process in massive stars at low metallicity: the effect of primary ^{14}N from fast rotating stars. Astrophys. J., **687**, L95–L98 (2008). doi: 10.1086/593350

[27] A. Choplin, R. Hirschi, G. Meynet, *et al.*, The intermediate neutron capture process. Astron. Astrophys., **618**, A133 (2018). doi: 10.1051/0004-6361/201833297

[28] J. J. Cowan, W. K. Rose, Heavy-element synthesis in the helium-burning cores of massive stars. Astrophys. J., **212**, 149–158 (1977). doi: 10.1086/155030

[29] T. Mishenina, M. Pignatari, G. Carraro, *et al.*, New insights on Ba overabundance in open clusters. Evidence for the intermediate neutron-capture process at play? Mon. Not. R. Astron. Soc., **446**, 3651–3668 (2015). doi: 10.1093/mnras/stu2337 arXiv: 1411.1422 [astro-ph.SR]

[30] I. U. Roederer, A. I. Karakas, M. Pignatari, F. Herwig, The diverse origins of neutron-capture elements in the metal-poor star HD 94028: possible detection of products of I-process nucleosynthesis. Astrophys. J., **821**, 37 (2016). doi: 10.3847/0004-637X/821/1/37 arXiv: 1603.00036 [astro-ph.SR]

[31] D. Karinkuzhi, S. Van Eck, S. Goriely, *et al.*, Low-mass low-metallicity AGB stars as an efficient *i*-process site explaining CEMP-rs stars. Astron. Astrophys., **645**, A61 (2021). doi: 10.1051/0004-6361/202038891 arXiv: 2010.13620 [astro-ph.SR]

[32] T. T. Hansen, J. D. Simon, T. S. Li, A. Frebel, I. Thompson, S. Shectman, Evidence for multiple nucleosynthetic processes from carbon-enhanced metal-poor stars in the Carina dwarf spheroidal galaxy. Astron. Astrophys., **674**, A180 (2023). doi: 10.1051/0004-6361/202346168 arXiv: 2305.02316 [astro-ph.SR]

[33] M. Hampel, R. J. Stancliffe, M. Lugaro, B. S. Meyer, THE INTERMEDIATE NEUTRON-CAPTURE PROCESS AND CARBON-ENHANCED METAL-POOR STARS. Astrophys. J., **831**, 171 (2016). doi: 10.3847/0004-637X/831/2/171

[34] K. Jonsell, P. S. Barklem, B. Gustafsson, *et al.*, The Hamburg/ESO R-process enhanced star survey (HERES). III. HE 0338-3945 and the formation of the *r* + s stars. Astron. Astrophys., **451**, 651–670 (2006). doi: 10.1051/0004-6361:20054470 arXiv: astro-ph/0601476

[35] S. Bisterzo, R. Gallino, O. Straniero, S. Cristallo, F. Käppeler, The role of binaries in the enrichment of the early Galactic halo - III. Carbon-enhanced metal-poor stars – CEMP-*s* stars. Mon. Not. R. Astron. Soc., **422**, 849–869 (2012). doi: 10.1111/j.1365-2966.2012.20670.x

[36] M. Lugaro, A. I. Karakas, R. J. Stancliffe, C. Rijs, Post-AGB stars in the Magellanic Clouds and neutron-capture processes in AGB stars. Astrophys. J., **747**, 2 (2012). doi: 10.1088/0004-637X/747/1/2

[37] C. Abate, R. J. Stancliffe, Z.-W. Liu, How plausible are the proposed formation scenarios of CEMP-*r/s* stars? Astron. Astrophys., **587**, A50 (2016). doi: 10.1051/0004-6361/201527864

[38] M. Hampel, A. I. Karakas, R. J. Stancliffe, B. S. Meyer, M. Lugaro, Learning about the Intermediate Neutron-capture Process from Lead Abundances. Astrophys. J., **887**, 11 (2019). doi: 10.3847/1538-4357/ab4fe8

[39] A. Choplin, L. Siess, S. Goriely, The intermediate neutron capture process. I. Development of the *i*-process in low-metallicity low-mass AGB stars. Astron. Astrophys., **648**, A119 (2021). doi: 10.1051/0004-6361/202040170 arXiv: 2102.08840 [astro-ph.SR]

[40] A. Choplin, L. Siess, S. Goriely, The intermediate neutron capture process. III. The *i*-process in AGB stars of different masses and metallicities without overshoot. Astron. Astrophys., **667**, A155 (2022). doi: 10.1051/0004-6361/202244095 arXiv: 2209.10303 [astro-ph.SR]

[41] A. Choplin, L. Siess, S. Goriely, S. Martinet, The intermediate neutron capture process. V. The *i*-process in AGB stars with overshoot. Astron. Astrophys., **684**, A206 (2024). doi: 10.1051/0004-6361/202348957 arXiv: 2402.10284 [astro-ph.SR]

[42] A. Choplin, L. Siess, S. Goriely, P. Eggenberger, F. D. Moyano, The intermediate neutron capture process: VI. Proton ingestion and *i*-process in rotating magnetic asymptotic giant branch stars. Astron. Astrophys., **706**, A44 (2026). doi: 10.1051/0004-6361/202557649

[43] K. De Smedt, H. Van Winckel, A. I. Karakas, *et al.*, Post-AGB stars in the SMC as tracers of stellar evolution: the extreme *s*-process enrichment of the 21 μm star J004441.04-732136.4. Astron. Astrophys., **541**, A67 (2012). doi: 10.1051/0004-6361/201219150

[44] K. De Smedt, H. Van Winckel, D. Kamath, *et al.*, A study of post-AGB stars in the Magellanic Clouds. I. The high-resolution optical spectra. Astron. Astrophys., **563**, L5 (2014). doi: 10.1051/0004-6361/201423721

[45] M. Lugaro, S. W. Campbell, H. Van Winckel, *et al.*, Post-AGB stars as tracers of AGB nucleosynthesis: the *s*-process in the Magellanic Clouds. Astron. Astrophys., **583**, A77 (2015). doi: 10.1051/0004-6361/201526759

[46] F. Herwig, M. Pignatari, P. R. Woodward, *et al.*, Convective-reactive nucleosynthesis and the origin of the neutron-rich isotopes beyond iron. Astrophys. J., **727**, 89 (2011). doi: 10.1088/0004-637X/727/2/89 arXiv: 1009.6087 [astro-ph.SR]

[47] F. Herwig, P. R. Woodward, P.-H. Lin, M. Knox, C. Fryer, The first three-dimensional simulations of carbon burning in a massive star. Astrophys. J. Lett., **792**, L3 (2014). doi: 10.1088/2041-8205/792/1/L3 arXiv: 1406.6688 [astro-ph.SR]

[48] L. Siess, M. Livio, J. Lattanzio, On the origin and evolution of the *s*-process elements in massive stars. Astrophys. J., **570**, 329–343 (2002). doi: 10.1086/339733

[49] S. W. Campbell, J. C. Lattanzio, The evolution of low-mass AGB stars: Nucleosynthesis yields and the impact of hot bottom burning. Astron. Astrophys., **490**, 769–776 (2008). doi: 10.1051/0004-6361:200810139

[50] M. Tian, W. Cui, J.-R. Shi, J.-X. Qin, H. Li, F. Wen, Z. Huo, Study of neutron capture nucleosynthesis based on post-asymptotic giant branch stars. Astrophys. J., **992**: 56 (2025). doi: 10.3847/1538-4357/ae03b5

[51] K. De Smedt, H. Van Winckel, D. Kamath, *et al.*, A study of post-AGB stars in the Magellanic Clouds. II. Chemical abundances of carbon-enhanced metal-poor post-AGB stars. Astron. Astrophys., **587**, A6 (2016). doi: 10.1051/0004-6361/201526929

[52] S. Cristallo, L. Piersanti, O. Straniero, *et al.*, Evolution, nucleosynthesis, and yields of low-mass asymptotic giant branch stars at different metallicities. III. Stellar yields and the *s*-process. Astrophys. J., **833**, 181 (2016).

[53] S. Cristallo, L. Piersanti, O. Straniero, *et al.*, The FRUITY database: A stellar evolution and nucleosynthesis portal. Astrophys. J., Suppl. Ser., **219**, 40 (2015).

[54] S. Cristallo, L. Piersanti, O. Straniero, *et al.*, Evolution, nucleosynthesis, and yields of low-mass asymptotic giant branch stars at different metallicities. II. The FRUITY database. Astrophys. J., **801**, 53 (2015).

[55] O. Straniero, S. Cristallo, L. Piersanti, *et al.*, Evolution and nucleosynthesis of asymptotic giant branch stars. I. The case of low-mass stars. Astrophys. J., **787**, 77 (2014).

[56] L. Piersanti, S. Cristallo, O. Straniero, *et al.*, Evolution and nucleosynthesis of asymptotic giant branch stars. II. The case of intermediate-mass stars. Astrophys. J., **774**, 98 (2013).

[57] S. Cristallo, O. Straniero, R. Gallino, *et al.*, Evolution, nucleosynthesis, and yields of low-mass asymptotic giant branch stars at different metallicities. Astrophys. J., **696**, 797 (2009).

[58] S. Cristallo, O. Straniero, R. Gallino, *et al.*, Evolution, nucleosynthesis, and yields of low-mass asymptotic giant branch stars at different metallicities. I. Stellar models and their nucleosynthesis. Astrophys. J., **667**, 489 (2007).

[59] O. Straniero, R. Gallino, S. Cristallo, *et al.*, *s*-Process in low-mass asymptotic giant branch stars. Nuclear Physics A, **777**, 311–334 (2006).

[60] D. Kamath, F. Dell'Agli, P. Ventura, H. Van Winckel, S. Tosi,

A. I. Karakas, Modelling of the Post-Asymptotic Giant Branch Phase as a Tool to Understand Asymptotic Giant Branch Evolution and Nucleosynthesis. Mon. Not. R. Astron. Soc., **519**, 2169–2185 (2022). doi: 10.1093/mnras/stac3366

[61] B. Meyer, in *Proc. XII Nuclei in the Cosmos Symp.*, ed. by J. Lattanzio *et al.* (Trieste: PoS, 2012)

[62] R. H. Cyburt, A. M. Amthor, R. Ferguson, *et al.*, The JINA REACLIB database: Its recent updates and impact on type-I X-ray bursts. Astrophys. J., Suppl. Ser., **189**, 240–252 (2010). doi: 10.1088/0067-0049/189/1/240

[63] M. Lugaro, A. I. Karakas, R. J. Stancliffe, C. Rijs, The *s*-process in asymptotic giant branch stars of low metallicity and the composition of carbon-enhanced metal-poor stars. Astrophys. J., **747**, 2 (2012). doi: 10.1088/0004-637X/747/1/2

[64] A. I. Karakas, A. F. Marino, D. M. Nataf, Nucleosynthesis in helium-enriched asymptotic giant branch models: implications for heavy element enrichment in omega centauri. Astrophys. J., **784**, 32 (2014). doi: 10.1088/0004-637X/784/1/32

[65] B. Paxton, L. Bildsten, A. Dotter, *et al.*, Modules for experiments in stellar astrophysics (MESA). Astrophys. J., Suppl. Ser., **192**, 3 (2011).

[66] B. Paxton, M. Cantiello, P. Arras, *et al.*, Modules for experiments in stellar astrophysics (MESA): Convective boundaries, element diffusion, and massive star explosions. Astrophys. J., Suppl. Ser., **208**, 4 (2013).

[67] B. Paxton, P. Marchant, J. Schwab, *et al.*, Modules for experiments in stellar astrophysics (MESA): Binaries, pulsations, and explosions. Astrophys. J., Suppl. Ser., **220**, 15 (2015).

[68] B. Paxton, J. Schwab, E. B. Bauer, *et al.*, Modules for experiments in stellar astrophysics (MESA): Convective cores, low-mass stars, stellar populations, and Kepler. Astrophys. J., Suppl. Ser., **234**, 34 (2018).

[69] B. Paxton, R. Smolec, J. Schwab, *et al.*, Modules for experiments in stellar astrophysics (MESA): Pulsating variable stars, rotation, convective boundaries, and energy conservation. Astrophys. J., Suppl. Ser., **243**, 10 (2019).

[70] A. S. Jermyn, E. B. Bauer, J. Schwab, *et al.*, Modules for experiments in stellar astrophysics (MESA): Time-dependent convection, energy conservation, and automatic differentiation. Astrophys. J., Suppl. Ser., **265**, 15 (2023).

[71] E. Huscher, K. Finlator, J. Jackiewicz, Asymptotic giant branch mass-loss rates and metal yields from scaled mixing-length and mass-loss parameters. Astrophys. J., **993**, 16 (2025). doi: 10.3847/1538-4357/ae0199

[72] N. R. Rees, R. G. Izzard, A. I. Karakas, Modelling binary population synthesis of post-AGB stars and planetary nebulae. Mon. Not. R. Astron. Soc., **527**, 9643–9663 (2024). doi: 10.1093/mnras/stad3758

[73] F. Herwig, The evolution of low-mass AGB stars. I. Evolution and nucleosynthesis to the end of the thermally pulsing phase. Astron. Astrophys., **360**, 952–968 (2000).

[74] E. Magg, M. Bergemann, A. Serenelli, *et al.*, Observational constraints on the origin of the elements. V. The chemical composition of the Sun re-analysed. Astron. Astrophys., **661**, A140 (2022). doi: 10.1051/0004-6361/202142971

[75] M. Asplund, N. Grevesse, A. J. Sauval, P. Scott, The chemical composition of the sun. Annu. Rev. Astron. Astrophys., **47**, 481–522 (2009). doi: 10.1146/annurev.astro.46.060407.145222

[76] C. Arlandini, F. Käppeler, K. Wisshak, *et al.*, Neutron capture in low-mass asymptotic giant branch stars: cross sections and abundance signatures. Astrophys. J. **525**, 886–900 (1999). doi: 10.1086/307938

[77] A. Choplin, S. Goriely, L. Siess, S. Martinet, Synthesis of actinides and short-lived radionuclides during *i*-process nucleosynthesis in AGB stars. Eur. Phys. J. A **61**, 68 (2025). doi: 10.1140/epja/s10050-025-01522-8

[78] N. Prantzos, C. Abia, S. Cristallo, M. Limongi, A. Chieffi, Chemical evolution with rotating massive star yields II. A new assessment of the solar *s*- and *r*-process components. Mon. Not. R. Astron. Soc. **491**, 1832 (2020).

[79] P. A. Denissenkov, F. Herwig, U. Battino, *et al.*, I-process nucleosynthesis and mass retention efficiency in He-shell flash evolution of rapidly accreting white dwarfs. Astrophys. J., **834**, L10 (2017). doi: 10.3847/2041-8213/834/2/L10

[80] P. Denissenkov, G. Perdikakis, F. Herwig, *et al.*, The impact of (n, γ) reaction rate uncertainties of unstable isotopes near N = 50 on the *i*-process nucleosynthesis in He-shell flash white dwarfs. J. Phys. G: Nucl. Part. Phys., **45**, 055203 (2018). doi: 10.1088/1361-6471/aabb6e

[81] P. A. Denissenkov, F. Herwig, P. Woodward, R. Andrassy, M. Pignatari, S. Jones, The i-process yields of rapidly accreting white dwarfs from multicycle He-shell flash stellar evolution models with mixing parametrizations from 3D hydrodynamics simulations. Mon. Not. R. Astron. Soc., **488**, 4258–4270 (2019). doi: 10.1093/mnras/stz1921